Wear 540-541 (2024) 205258

Contents lists available at ScienceDirect

Wear

journal homepage: www.elsevier.com/locate/wear

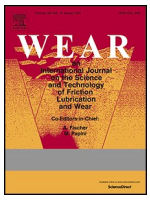

Enhancing wear performance: A comparative study of traditional vs. additive manufacturing techniques for 17–4pH SS

Celia García-Hernández [a], Juan Alfonso Naranjo [b], María Ángeles Castro-Sastre [c], Cristina Berges [b], A.I. Fernandez-Abia [c], Fernando Martín-Pedrosa [a], Gemma Herranz [b,**], Cristina García-Cabezón [a,*]

[a] Universidad de Valladolid, Escuela de Ingeniería Industriales, BioEcouva. C/Paseo Del Cauce N° 59, 47011, Valladolid, Spain
[b] Universidad de Castilla–La Mancha, INEI-Escuela Técnica Superior de Ingeniería Industrial, Av. Camilo José Cela s/n, 13071, Ciudad Real, Spain
[c] Department of Mechanical, Informatics and Aerospace Engineering, Universidad de León, Campus de Vegazana, 24071, León, Spain

ARTICLE INFO

Keywords:
17-4pH SS
Selective laser melting (SLM)
Fused filament fabrication (FFF)
Lubrication
Tribology

ABSTRACT

This study investigates the microstructural, mechanical, and tribological characteristics of 17–4 PH stainless steel specimens produced through Additive Manufacturing (AM) techniques, namely Selective Laser Melting (SLM) and Fused Filament Fabrication (FFF), in comparison to conventionally wrought steel (W). The wear test carried out on the samples were pin-on-disk, ball-on-plate and lubricated pin-on-disk. The counter part was an alumina ball with a diameter of 3 mm. The wear scar was less pronounced on lubrication test than in dry conditions for all samples. The coefficients of friction (COFs) were higher in dry conditions (in the order of 10^{-1}) than in lubrication conditions (in the order of 10^{-2}). Moreover, the wear rate had a significant reduction under lubrication conditions (in dry tests are in the order of 10^{-7}, while lubrication conditions led to results in the order of 10^{-9}). Additionally, FFF and SLM exhibited remarkably low wear rates in comparison to the wrought sample showing a superior dry and lubricated wear behaviour. AM allows for comparable or improved properties, despite slightly lower hardness due to retained austenite/delta ferrite and reduced precipitates. That significant improvement enhances the appeal of AM for high-performance components, particularly for small production runs and complex geometries being a promising and efficient technology for diverse industries.

1. Introduction

The precipitation-hardened martensitic stainless steel 17-4 PH (UNS S17400) is renowned for its exceptional strength and corrosion resistance [1]. This material is in high demand across diverse industries such as marine, petrochemical, nuclear, and aerospace sectors [2,3]. However, the challenge in working with 17-4 PH lies in its formidable properties, stemming from precipitation hardening, which complicates traditional machining. As a result, 17-4 PH has typically been used in its conventional wrought form with an established processing history.

A novel approach has emerged through Additive Manufacturing (AM) technologies, enabling rapid, cost-effective production of intricate 17-4 PH parts while minimizing post-processing requirements [4]. Notably, 17-4 PH is the second most used material in metal material extrusion (MEX) after 316L alloy [5].

Comparing conventional and advanced methods, traditional wrought processes involve controlled deformation under high pressure and temperature, providing a well-established technology [6]. In contrast, AM offers greater design freedom and customization, facilitating complex geometries and lightweight components that are economically unviable with traditional methods [7]. AM is not limited to prototyping and has seen substantial growth in various applications, including end-use parts [5].

AM involves the layer-by-layer fusion of materials based on 3D models, offering a contrast to subtractive manufacturing methods. Metal fabrication using Fused Filament Fabrication (FFF) is an indirect AM technique belonging to MEX, sharing similarities with Metal Injection Molding (MIM) [5]. It relies on debinding and sintering processes to achieve desired properties, providing intricate components and multi-material capabilities with reduced lead times and material waste.

* Corresponding author.
** Corresponding author.
E-mail addresses: gemma.herranz@uclm.es (G. Herranz), crigar@uva.es (C. García-Cabezón).

https://doi.org/10.1016/j.wear.2024.205258
Received 3 November 2023; Received in revised form 25 December 2023; Accepted 11 January 2024
Available online 14 January 2024

On the other hand, Selective Laser Melting (SLM), a direct AM technique based on powder bed fusion, employs a high-energy laser to selectively melt and fuse powder particles layer by layer, enabling the fabrication of complex geometries in less time than FFF. However, challenges include residual stresses, thermal cracks, and anisotropy [8,9].

The distinction between these methods is that SLM is direct, requiring no post-processing after the printing stage, but it is costlier and demands 100 % infill density unless an open structure is used. FFF may have a coarser surface finish but offers superior design flexibility, interlayer support structures for part separation, and customizable infill density, reducing raw material consumption and weight [10].

Carbon and nitrogen content control is essential in the manufacturing process, significantly affecting the final properties of 17-4 PH parts, having a significant influence on both mechanical properties and corrosion resistance, being necessary a compromise between both factors. Regarding powder atomization conditions, argon-atomized powder consistently results in a martensitic phase, while nitrogen-atomized powder contains higher nitrogen content, leading to austenitic phases and impacting mechanical properties [11–13].

The microstructural differences between AM and wrought components can be substantial [14]. In addition, interstitial defects, together with porosity, which plays a crucial role in determining mechanical properties of FFF and SLM parts, can contribute to significant variations in the properties of the fabricated parts [15,16]. The typical heat treatment procedure for conventionally wrought 17-4 PH involves homogenization and aging treatments, resulting in a fully martensitic matrix along with coherent Cu-rich precipitates in a body-centered cubic (BCC) structure. On the other hand, the rapid solidification process involved in SLM often leads to a predominantly martensitic microstructure with dendritic structure in the as-built condition [13,17]. In the case of as sintered FFF 17-4 PH, specific defects such as porosity, lack of fusion, and delamination between build layers may be present, which are not typically found in wrought materials [18].

The influence of the processing method on the microstructure directly affects the mechanical properties of the formed parts. Despite the large amount of recent research conducted on AM 17-4 PH, most research carried out on specimens fabricated by FFF [19–21] and SLM [11,17,22] are based on the influence of printing parameters on final properties, in terms of final density, microstructure and tensile behaviour, however, very few articles have studied the tribological behaviour of 17-4 PH parts processed by these AM technologies [23,24]. Sanjeev et al. [25] have stated that LB-PBF 17–4 PH specimens have lower dry wear rate than the wrought one. More recently, Naim et al. [26] have studied the tribological properties of 17-4 PH parts processed by FFF, showing that the surface porosity is a key factor in the tribological performance, inducing stress concentrations that lead to material wear via abrasion and adhesion. In the same context, Sanguedolce et al. [27] have studied the effect of surface texture on SLM printed samples, obtaining a significant increase of the Coefficient of friction (COF) in the textured samples with respect to the as-produced samples. Parallelly, Li et al. [28] have stated that despite the microstructural heterogeneity associated with SLM-processed, the build-up directions do not have a noticeable influence on friction and wear properties on the steel. Tekdir and Yetim [29] have also focused on the tribological study of stainless steels, specifically on 316L processed by SLM. In this work, they describe that the 316L samples undergo intense plastic deformation and delamination processes. In this case, the authors went further by seeking to enhance the material through the application of coatings on its surface.

In the present study, three technologies are applied to produce 17-4 PH parts, as a way to highlight the role of manufacturing processing in microstructure and mechanical properties in terms of hardness, wear and flexural strength, highlighting the importance of selecting the right technology based on part geometry and intended application.

2. Experimental

2.1. Samples under study

The tribological and mechanical behaviour of 17–4 PH SS additively manufactured using SLM and FFF is compared to its commercial wrought counterpart. For this purpose, the SLM and FFF samples under study were X–Y planes, perpendicular to the built direction. The surface of the samples was prepared by grinding with silicon carbide abrasive papers up to 1000 and by polishing with diamond suspension (6 μm and 1 μm). The etching of samples was carried out using Vilella, Fry and oxalic acid solutions.

Commercial 25 mm diameter bar (from BGH Edelstahl Freital GmbH) formed by hot plastic deformation and heat treated is used as reference material, Wrought 17–4 PH SS. The chemical composition is shown in Table 1. The solution heat treatment was performed at 1040 °C for 130 min, followed by air cooling to room temperature. The ageing treatment is carried out in two steps: 625 °C for 7h and 630 °C for 9.5 h, with air cooling to room temperature.

In the FFF process, the printing requires the use of a binder system. The employed binder system consisted of a combination of thermoplastic polymers and additives, which has been proven to enable robust processing of 17-4 PH [30], ensuring the consolidation of the desired geometries. A mixture of 60 vol% metallic powder (Table 1) and the binder system was prepared using a ThermoHaake double rotor mixer (Haake Rheocord 252p model) working at 40 rpm and 220 °C for 70 min. Then, filaments were produced using a single screw extruder equipped with a heater, ranging from room temperature up to 300 °C. The filaments were extruded at temperatures within the range of 150–170 °C and wound onto spools, resulting in filaments with a diameter of 1.75 ± 0.06 mm. Subsequently, the printing process was conducted using a conventional filament machine (3D Prusa Steel Black Edition Mark II) and the printing parameters provided in Table 2. An in-depth study evaluating the influence of these parameters on the rheological properties of the material during printing was previously evaluated [30].

Once the green parts were obtained, the debinding process was performed in two stages. The first step involved using an organic solvent in a digital thermostatic bath (OVAN B105-DE), while the second step involved programmed thermal cycles in a Carbolite CWF 11/13 furnace under a N_2 atmosphere. Following the debinding steps, the brown parts were sintered at 1380 °C in a tubular Carbolite STF 15/450 furnace under vacuum. The heating rate was set at 5 °C/min until reaching the maximum sintering temperature, which was maintained for 1 h. Finally, the parts were cooled inside the furnace.

SLM samples were cubic specimens with dimensions 10x10 × 10 mm. The samples were printed using a Direct Metal Printing ProX 100 SLM machine (3DSystems). The main printing parameters that influence the properties and quality of the parts are laser power, scanning speed, layer height, scanning strategy and hatch spacing. The values set for these parameters are specified in Table 2. These values have been chosen based on the recommendations provided by the machine manufacturer and the supplier of the metallic powder. These values ensure the production of parts with maximum density and minimal defects. The printing process was carried out in a nitrogen protective atmosphere. Samples were printed from recycled powder as usual in this process for cost effectiveness. Table 1 shows the chemical composition of the recycled powder. It can be seen that the oxygen content is slightly higher due to the recycling process. The nitrogen content is also higher because the printing process is carried out in a chamber with inert nitrogen gas.

2.2. Microstructural characterization

Microstructural characterization was carried out using optical microscopy (OLYMPUS BX53 M) and scanning electron microscopy with energy dispersive X-ray spectroscopy (SEM/EDS) (QUANTA 200F, FEI).

Table 1
Chemical composition of 17–4pH SS specimens under study.

Elements	C	Cr	Ni	Mo	Mn	Si	Cu	Nb	N	S	O	Fe
Wrought	0.032	15.70	4.30	0.15	0.61	0.27	3.13	0.25	0.004	0.0005	0.009	Bal.
SLM	0.026	16.93	4.17	0.05	0.58	0.62	3.56	0.21	0.083	0.0004	0.0857	Bal.
FFF	0.067	16.1	3.92	0.08	0.19	0.69	3.66	0.19	0.06	0.0003	0.0169	Bal.

Table 2
Printing parameters of FFF and SLM processing technologies.

Processing technology	Nozzle diameter (mm)	Layer height (μm)	Hatch spacing (μm)	Scanning/Printing speed (mm/s)	Nozzle temperature (°C)	Platform temperature (°C)	Laser power (W)	Printing strategy
SLM	–	30	70	140	–	–	38	Hexagonal
FFF	0.4	200	–	25	250–270	60	–	Rectilinear

Phase analysis were made using X-ray difraction (XRD) (Bruker Discover D8 and Agilent SuperNova) to obtain the patterns of the samples and wear debris. The identification of the phases was accomplished using Diffrac EVA software. The characterization of somesamples has been published with detailed description in a previous work [31]. Moreover, after carrying out the wear test, the samples were observed by optical microscopy and SEM with EDS to study the wear mechanism on the 17–4 PH samples surfaces.

2.3. Mechanical characterization

A Centaur 920 Durometer was used to carry out measurements of Vickers macrohardness with 30 kg for 30 s according to ISO 6507–1. Additionally, microhardness was measured using a Matsuzawa MXT70 applying 100 g load during 30 s in order to consider the influence of the porosity of the additive manufactured samples in the hardness characterization. For each hardness test, at least ten measurements were taken in different locations of the top surface of the 17–4 PH SS samples and means and standard deviations of the test were calculated.

Three-point tests are performed on metallic final parts with rectangular geometry (66x12 × 4.5 mm), These tests are performed on a Shimadzu model Autograph AG-X 50 KN, applying increasing loads on the perpendicular of the specimen by a uniform rectilinear movement of 1 mm/min, and recording the displacement and load values.

2.4. Wear tests

Rotating pin-on-disk wear tests were carried out using a pin-on-disk tribometer at room temperature following ASTMG99 standard under both dry and lubricate sliding conditions, mineral oil as used as lubricant. Moreover, the behaviour of the samples showed in the dry pin-on-disk test were compared with that performed by dry linear reciprocating test (ball-on-plate). For this purpose, before the wear tests, the surface of the specimens was prepared by grinding with SiC abrasive papers up to 1000, and afterwards, cleaned for 5 min with acetone in an ultrasonic bath. The counter part was an alumina ball with a diameter of 3 mm and Vickers hardness of 1500–1650. The conditions of the tests were selected based on previous tribological studies [29] and they are as follows in Table 3.

All tests were carried out at least five times to ensure reliability and in order to obtain statistical measures (mean and standard deviation). During the test, the coefficient of friction (COF) was continuously recorded against the sliding distance. After the tests, the morphology of the wear scar was observed by optical microscopy to measure the width of the scar using image analysis and by SEM/EDX to obtain information regarding the wear mechanisms and chemical composition of the wear scar. The resultant wear track profiles were examined using a SJ-500P profilometer with a stylus radius of 2 μm. Three measurements were made for each specimen and the depth of the worn groove was measured from the profile. The result for the depth of the wear track of each specimen were averaged.

The resultant wear track profiles were examined by a profilometer to assess the general features of the wear track. The wear volume loss was calculated according to the ASTMG99 standard [32] in the case of the dry and lubricate pin-on-disk tests and following ASTMG133 standard [33] for the reciprocating test. The wear rates were calculated using the conventional expression:

$$Wear\ rate\ \left(mm^3 \cdot N^{-1} \cdot m^{-1}\right) = \frac{Volume\ loss\ (mm^3)}{Normal\ load\ (N) \cdot Sliding\ distance\ (m)} \quad \text{Eq. (1)}$$

Additionally, XRD spectra of the debris removed during testing was carried out in order to observe the identification of the phases. Finally, the loss of material for the alumina counter-body in tests was found insignificant and, moreover, some debris was observed on the alumina ball after each test.

3. Results and discussion

3.1. Microstructural characterization

Fig. 1 shows the differences in the microstructure of the 17–4 PH SS samples. As reported before, the 17–4 PH SS wrought sample showed a martensite matrix with small areas of retained austenite with no evidence of islands of delta-ferrite while the microstructure of SLM 17–4 PH SS was clearly more heterogeneous and the most important microstructural characteristics were the overlapping hemispherical melt pools due to the laser track in the normal orientation to the build direction. The SLM samples are generally free of defects and might show small pores and non-metallic inclusions. Moreover, dendritic segregation across the melt pools was observed in the SLM samples caused by the high rates of cooling [31]. FFF sample showed a duplex microstructure, with microconstituents identified as delta-ferrite (light grey) island in a martensitic matrix (dark grey). Additionally, the dark regions are oxide

Table 3
Wear test conditions for tribological studies of 17–4pH SS samples.

Wear test	Normal load applied (N)	Sliding velocity (m/s)	Sliding distance (m)	Track radius (mm)	Sliding stroke (mm)
Dry pin-on-disk	5	0.05	200	3	–
Dry linear reciprocanting	5	0.05	500	–	10
Lubricate pin-on-disk	5	0.05	500	3	–

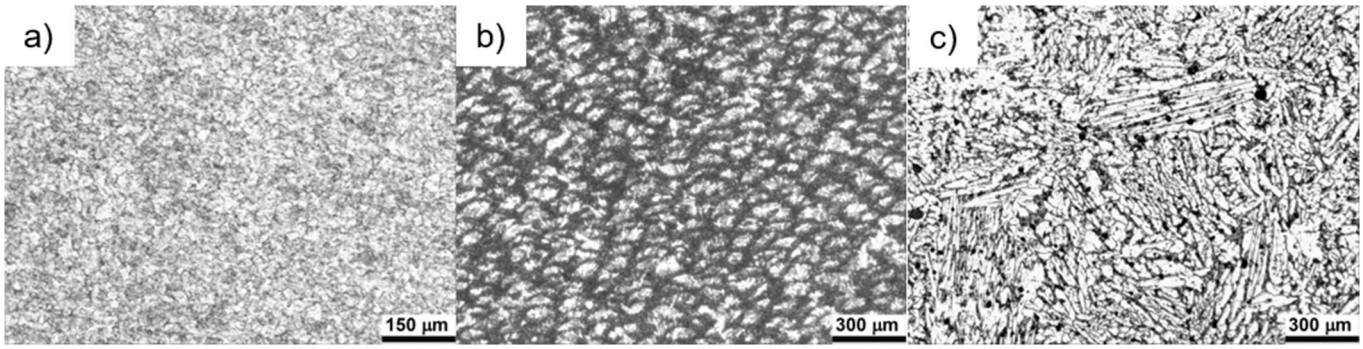

Fig. 1. Optical microstructure of a) Wrought, b) SLM and c) FFF samples, after etching.

inclusions and pores. This ferritic structure is caused by the high heating and cooling rates, that prevents the formation of austenitic structure (and initial delta ferrite cannot be transformed).

The microstructural features observed by optical microscopy was confirmed by the XRD spectra analyses. The results have been discussed in previous research works of the authors [25]. The most important peaks correspond to the BCC phase associated with martensite or delta ferrite, although it is difficult to distinguish between both from the XRD patterns. However, based on the micrographs and XRD results obtained as well as in the reported literature, it has been established that the wrought sample showed a fully martensitic microstructure with retained austenite due to the presence of austenite-stabilizing elements (i.e. Cu or Ni) that decrease the martensite start temperature transformation [34]. In the case of additive manufacturing samples, it is important taking into account the presence of nitrogen in the manufacturing process that acts as an austenite-stabilizing element allowing the formation of austenite and later the transformation of austenite to martensite. Additionally, the high heating and cooling rates are also of importance in this phase transformation since do not allow the austenite formation from delta ferrite and subsequently a ferritic microstructure is predominant. Therefore, both facts, the nitrogen content and high heating and cooling conditions, will compete in the phase transformation.

In the case of the SLM sample, the higher content of nitrogen leads to the transformation of delta ferrite to austenite which, in turn, is transformed into martensite during the rapid cooling. Moreover, the presence of austenite stabilizing elements (i.e. nitrogen) produce a decrease in the martensite start temperature causing the incomplete martensite transformation leaving austenite retained in the microstructure [31]. On the other hand, FFF samples showed a lower content of nitrogen than in SLM samples which means that delta ferrite is not fully transformed into austenite due to the high heating and cooling rates and, finally, this fact reduces the amount of martensite in the microstructure when comparing with the SLM sample. These results were later confirmed by the hardness measurements. Finally, the analysis of the XRD spectra confirmed the presence of retained austenite and some Nb–Cr precipitates in all the samples.

The microstructure of the 17–4 PH SS samples was further studied by SEM which revealed the presence of fine Nb-rich phases (Fig. 2). In the case of the wrought samples, it was observed light and small precipitates on the edges of the martensite plates and large inclusions dispersed in the matrix. In the SLM samples, small and spherical shape particles of precipitates were observed inside the melt pools and were more visible along the dendritic boundaries. In both cases, the small size of these precipitates did not allow to be analyse by EDS, however, the increase in Nb and Cr content was clear in these areas. Moreover, these results are consistent with the work reported by other authors [13]. Additionally, the wrought samples showed a higher content of inclusions when comparing to SLM samples that could be caused by the higher cooling rate in SLM samples fabrication that leads to an insufficient time for the nucleation process.

In the case of FFF samples, the SEM micrographs revealed the presence of a duplex microstructure with a continuous ferritic network in a martensitic matrix. The EDS analysis showed that the ferritic colonies were rich in Cr and Nb content while the martensitic matrix had a higher Ni and Cu content. Moreover, some precipitates were also observed at the boundaries of the delta ferrite colonies (light particles) and inside them (dark precipitates). Again, precipitates could not be analysed by EDS due to their small size but the increase in Nb and Cr content in the light precipitates was also confirmed. Dark non-metallic inclusions identified as oxides were also observed in all the samples with a predominant presence in the FFF samples. Finally, and although due to their small size were not possible to identify it typical Cu-rich precipitates

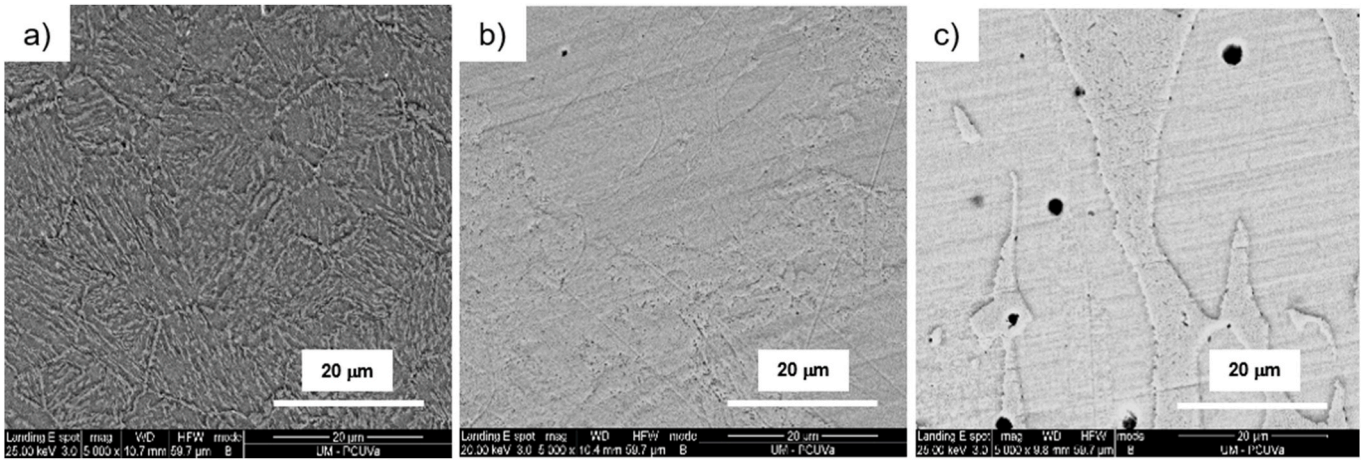

Fig. 2. SEM images showing the microstructure of a) Wrought, b) SLM and c) FFF samples.

would be expected to be present.

3.2. Mechanical characterization

The tests of the macro and micro hardness carried out in the samples confirmed the above results. Fig. 3 shows the Vickers hardness values of both for each sample. As expected, the porosity plays an important role in the determination of hardness. For example, in porous samples, such as the conventional PM, the macrohardness values are lower than the microhardness values due to the effect of porosity. Therefore, it can be stated that the higher the porosity, the lower the macrohardness. The microhardness measurements would give an idea of the intrinsic hardness of the materials without the influence of the pores and therefore the microhardness values are higher than the obtained in the macrohardness test in porous materials [35]. In this study, the macrohardness values are similar to that observed in microhardness tests, confirming that the degree of the porosity of the samples is very low. Moreover, the tendency in both tests were similar which also corroborated the martensitic microstructure observed before. The higher hardness was obtained in wrought samples, followed by the SLM samples and, finally, the FFF samples. In this study, it is important to highlight that the samples were obtained from different manufacturing processes and treatment conditions. Specifically, the SLM and FFF samples were analysed in their "as-built" conditions, while the wrought samples underwent the typical heat treatment employed during the fabrication process.

It is well known that heat treatment leads to the precipitation of Cu-rich nanoprecipitates which play an important role in the increase of the hardness in the thermal treated 17–4 PH SS by hindering the dislocation movements and producing a semi-coherent interface [36,37]. Moreover, the amount of austenite phase observed in SLM and FFF samples was higher than in the wrought sample and, as it is known, the austenite phase has influence in the mechanical properties reducing the hardness [38].

To further characterize the mechanical properties, bending measurements were carried out on standardised specimens (66x12 × 4.5 mm). Fig. 4 shows representative 3-point bending curves for wrought, SLM and FFF specimens, while Table 4 shows the most significant values of the bending tests. The results indicate that SLM specimens have the lowest values of yield strength (1280 MPa), followed by wrought (1370 MPa), while FFF specimens have the highest values (1520 MPa). By contrast, the flexural strength values are very similar in all three cases. These results show significant differences in deflection and yield strength, which may indicate that they are not mechanically equivalent.

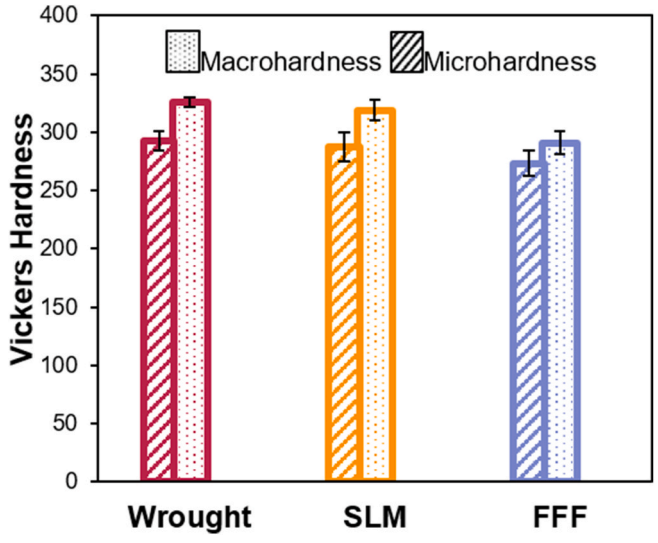

Fig. 3. Vickers hardness values of wrought, SLM and FFF samples.

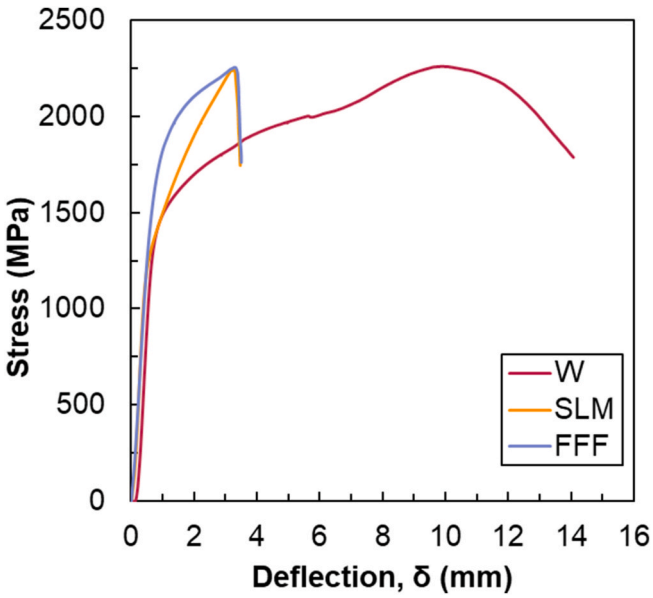

Fig. 4. 3-Point bending curves for wrought, SLM and FFF specimens.

Table 4
Detailed results obtained in the bending tests of 17–4pH SS samples.

Processing technology	Yield strength (MPa)	Flexural strength (MPa)	Deflection, δ (mm)
W	1370 ± 20	2300 ± 100	13.5 ± 0.9
SLM	1280 ± 20	2200 ± 100	3.2 ± 0.5
FFF	1520 ± 10	2100 ± 100	2.7 ± 0.8

Mechanically, the martensitic phase is expected to exhibit higher strength, yield strength, and lower elongation compared to the delta ferrite [17]. Microstructural analyses reveal a greater presence of martensitic phase in wrought and SLM samples compared to FFF. Surprisingly, bending test results show that FFF specimens exhibit higher yield strength and lower elongation. However, it is important to consider that although martensite is known for its strength, its initial yielding often occurs at low stresses due to residual intra-granular stresses from the transformation from austenite to martensite. Additionally, the presence of retained austenite alongside martensite in the samples, being a much softer phase, may affect the phase [39]. Deformation behaviour during tests exhibits significant differences among the specimens processed using the three different techniques. SLM and FFF show reduced and similar deflection values (3.2 mm and 2.7 mm, respectively), resulting in specimen fracture after this displacement. In contrast, wrought specimens display much higher values (13.5 mm), withstanding substantial deformation without fracturing. Surface roughness or isolated printing defects influence negatively SLM and FFF specimens, leading to higher stress concentrations and premature part failure. Moreover, the aging treatment leads to enhance ductility in the specimens.

3.3. Wear tests

Wear studies on 17–4 PH SS produced through additive manufacturing (AM) are currently limited in scope, with a predominant focus on fusion techniques. Comparative investigations of various AM techniques, such as Selective Laser Melting (SLM) and Fused Filament Fabrication (FFF), are particularly lacking in the existing literature. Addressing this research gap, the primary objective of this study is to conduct a comprehensive wear analysis of 17–4 PH steel processed via different AM techniques. By comparing the wear behaviour of SLM and

FFF samples, this research aims to provide valuable insights into the tribological performance of AM-produced components, contributing to a better understanding of their suitability and potential applications in real-world scenarios. However, previous studies on this topic have demonstrated that the build-up directions in Selective Laser Melting (SLM)-processed 17–4 PH steel do not significantly influence friction and wear properties [28]. In light of this, for the tribological tests on SLM samples, the cross-section normal to the direction of construction was chosen. Similarly, the cross-sections of Fused Filament Fabrication (FFF) and conventionally wrought samples were also examined to provide a comprehensive understanding of their tribological behaviour. This research aims to gain insights into the effects of manufacturing processes on the wear characteristics of 17–4 PH steel components, facilitating informed decision-making for their practical applications.

Regarding the test conditions, one of the features that mostly influence in the wear results is the hardness difference between the pin and the sample, being the wear greater when the hardness difference between both enhances [40]. In this study, the hardness of the alumina pin is quite higher than that from the specimens in order to promote severe wear conditions and to disregard the pin wear. Moreover, this selection also allows choosing low normal loads of 5 N and reduced sliding distances in order to avoid an excessive wear on the samples. Additionally, the selected sliding distance in the dry pin-on-disk test was smaller due to the higher wear obtained on the steel in comparison with the other two tests carried out (reciprocating test and lubricate circular test).

As stated before, three different sets of disk-shaped plates have been prepared for the tribological tests: SLM, FFF and Wrought. The SLM and FFF samples wear tests provide an assessment of the tribological behaviour of the as-printed steel, while the wrought sample, which has the conventional hardening heat treatment process, is used as the reference. Heat treatment has not been carried out on samples obtained by additive manufacturing for two reasons. Firstly, because of the economic advantage of eliminating secondary operations in the processing and, secondly, prior studies had proven that the conventional heat treatment is not very effective and leads to the formation of carbides, which could have adverse effects on the wear resistance [23]. The coefficients of friction (COF) vs. the sliding distance registered during the wear tests for each sample are shown in Fig. 5.

Fig. 5 a) shows the evolution of the dynamic COF during the pin-on-disk test and Table 5 shows the average COF of the last 50 m. In all samples, different stages for the COF during the sliding distance are observed. In the first stage the COF rises to a certain value and drops rapidly (due to the filing of material roughness) and then, it rises again and, finally, reaches a steady-state value. In addition, typical stick-slip oscillations were observed in the friction profiles of the samples. These oscillations are caused by a loss of energy and could be indicative of significant plastic deformations in the material and the phenomenon of micro-welding. The steady-state condition was reached earlier in the FFF sample and also showed less local fluctuations. However, the COFs at the end of the wear tests are similar for all three samples, although the SLM sample showed a slightly low value of COF.

Table 5
Average COF.

Wear test	W	SLM	FFF
Dry pin-on-disk	8.81E-01	8.08E-01	8.64E-01
Dry linear reciprocanting	7.95E-01	7.56E-01	8.06–01
Lubricate pin-on-disk	9.48E-02	7.48E-02	5.62E-02

The reciprocating wear tests were used to analyse the influence of processing method on tribological behaviour of 17–4 PH SS under different wear condition but using the same counter ball and the applying the same normal load. However, the sliding distance was higher (500 m instead of 200 m) due to the lower wear observed on the samples. In Fig. 5 b), it can be observed that the resulted static COF was similar than the dynamic COF registered by the pin-on-disk test and, once again, the SLM sample showed a lower COF value. The COF values under lubrication conditions are collected in Fig. 5 c), which clearly evidences in all samples the expected role in the notable decrease of COFs due to the lubrication. In this case, although all samples have very low coefficients of friction, the FFF sample has the highest frictional resistance under lubricated conditions. The wear scar was less pronounced on lubrication test due to the reduced static friction, less heat generated during testing and the lower traction components during wear. These results are in accordance with the literature since it is well known that lubricants can drastically change the friction and wear properties [41].

After the wear tests, the resultant wear scar width was measured using image analysis and the wear volume loss during testing was determined following ASTM G99 [32] and ASTM G133 [33]. The specific wear rates, which were calculated following Eq. (1), are shown in Fig. 6. As can be seen, SLM and FFF samples exhibited lower wear rates compared to the wrought sample in all tribological conditions and, therefore, indicating that the additively manufactured steels are more resistant to wear than the conventional steel. Furthermore, transitioning from dry to lubricated conditions led to a significant reduction in wear rate for all samples. While the difference between FFF and SLM wear rates became less pronounced in lubricated conditions, all samples exhibited remarkably low wear rates in comparison to the wrought sample.

Fig. 7 shows a typical profile of a worn groove corresponding to the disk-on-disk test for three different samples. It can be observed that the profile with the greatest depth corresponds to the wrought sample, while the SLM sample shows the shallowest depth. These observations underscore the potential benefits of additive manufacturing techniques in enhancing the wear performance of 17–4 PH steel components in various operating conditions.

Fig. 8 illustrates the depth of the worn grooves for SLM, FFF, and conventionally wrought 17–4 PH stainless steel. Remarkably, both SLM and FFF samples exhibited significantly lower depths of worn grooves across all tribological conditions, underscoring their superior wear

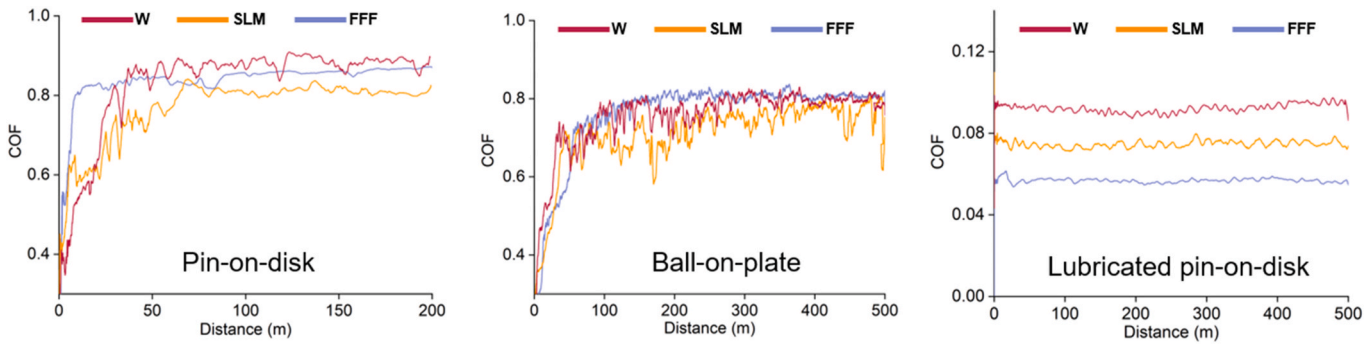

Fig. 5. Representation of the COF vs. distance obtained in the wear tests carried out on the samples.

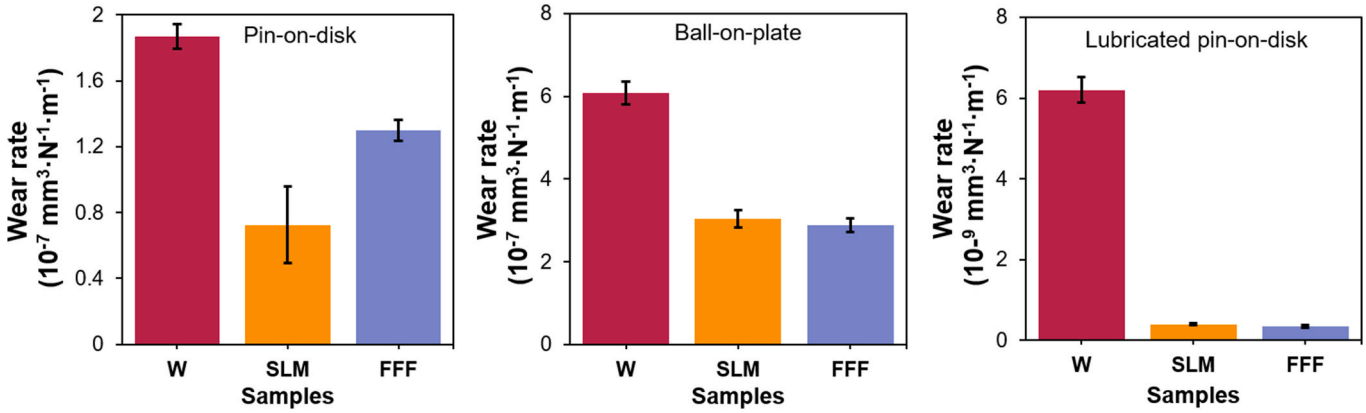

Fig. 6. Results of the wear rates obtained in the wear tests.

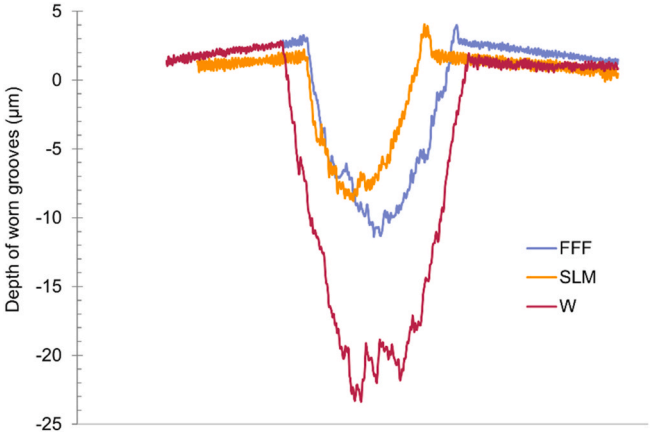

Fig. 7. Typical wear groove profile pin-on-disk test for three samples.

resistance compared to the wrought sample. These findings are in alignment with the observations made in the preceding paragraph, reinforcing the notion that both additive manufacturing techniques yield components with substantially reduced wear rates compared to their conventionally manufactured counterparts.

Therefore, it can be concluded that, for all three tribological conditions, the additive manufactured samples have shown a higher wear resistance than the conventional ones. The same conclusion was reached by Sanjeev et al. on 17–4 PH SS processed by laser-based additive manufacturing [25]. However, in that study this improvement is only observed under dry wear conditions, while the opposite is observed under lubricate conditions. In order to explain this difference, they suggested that the lubricant film is thinner on the additive manufactured samples due to the higher surface roughness. In the present study, all samples underwent the same surface preparation process, resulting in comparable surface roughness, thus negating surface roughness as a differentiating parameter. This suggests that the enhanced wear resistance observed in the additively manufactured samples can be attributed to other factors, such as microstructural characteristics and intrinsic material properties.

In comprehending the wear test results, it becomes evident that factors beyond hardness significantly influence wear resistance behaviour. Thus, despite the slightly higher hardness of the wrought sample (with hardening heat treatment), this factor does not mean that the wrought material has a better wear resistance. For example, as can be seen, in dry circular wear conditions, the wear rate of the SLM sample is almost three times lower than that obtained for the wrought sample and practically ten times lower in lubricated conditions. These distinctions can be attributed to the anisotropic microstructure of additively manufactured components, which differs from conventional stainless steel. Furthermore, the lower wear resistance of the wrought sample (which has a slightly higher hardness) is attributed to the higher amount of chromium/niobium precipitates that can be detached during the wear test and promote abrasive wear through the third body mechanism. On the other hand, the higher ferrite content in the Fused Filament Fabrication (FFF) sample, and consequently its lower hardness, contributes to lower wear resistance compared to the Selective Laser Melting (SLM) sample in the dry pin-on-disk test. However, this disparity diminishes under lubricated conditions and in the reciprocating wear test. In addition, for the SLM sample, the direction of the columnar grains with respect to the reciprocal direction is also important. In this study, the sliding direction is perpendicular to the columnar grains and according to Yang et al. this provides a lower sliding wear resistance by causing delamination of the oxide films [24]. In addition, the reciprocal wear rates of the as-printed sample were lower than those found in the literature for the SLM heat treated [23]. This confirms that the “as-built” condition is adequate for the additive manufacturing process without a

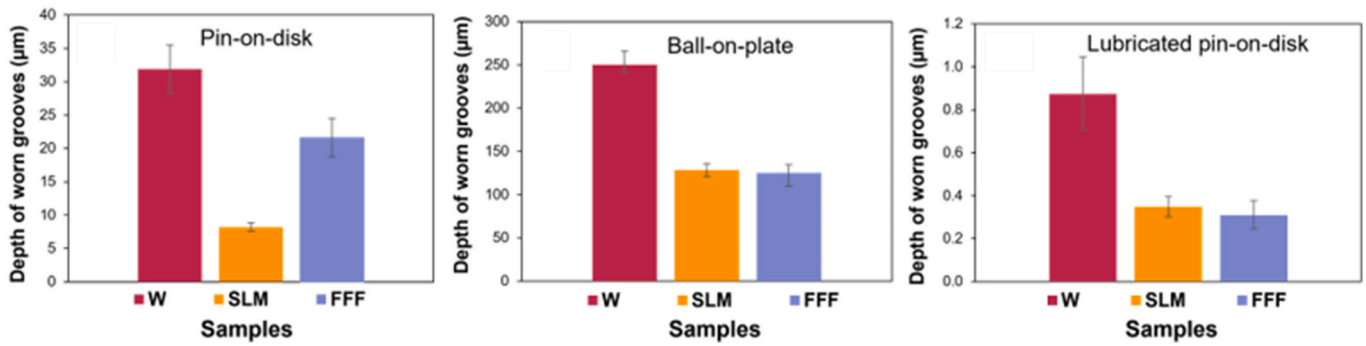

Fig. 8. Results of the depth of worn grooves obtained in the wear tests.

hardening heat treatment. The interplay of microstructural factors, hardness, and lubrication conditions significantly influences the wear behaviour of the samples, underscoring the complex nature of wear resistance in additively manufactured components.

3.4. Wear mechanism

These results emphasize the significance of microstructural characteristics unique to additive manufacturing, which play a pivotal role in enhancing wear performance. The impact of the wear tests was evaluated by examining the wear tracks using SEM-EDX analysis (Figs. 9–11). This examination involved assessing the width, morphology and composition of the wear tracks. Based on these data, the wear mechanism was discussed by comparing the worn surfaces of samples fabricated using different processes: additive manufacturing (FFF and SLM) and conventional manufacturing, under the three studied wear conditions.

In general, samples subjected to dry circular wear exhibited wider and more defined wear tracks compared to samples under lubricated circular wear, regardless of the manufacturing process employed. Samples fabricated using the conventional method demonstrated wider circular wear tracks than those produced using additive manufacturing.

Furthermore, noteworthy distinctions were observed in the wear track characteristics among the different manufacturing processes. Under dry wear conditions, SLM samples displayed narrower wear tracks, while FFF samples exhibited narrower tracks when lubrication was present. A similar trend was observed in the ball-on-plate test, mirroring the findings from the dry pin-on-disk test. In terms of wear track width, the following relationship was established: Wrought > FFF > SLM. These findings provide valuable insights into the wear behavior of the 17-4 PH material under various tribological conditions and shed light on the influence of different manufacturing processes on wear track formation. As discussed earlier, these results underscore the influence of the manufacturing process on wear resistance, as it can provide greater resistance under specific wear and fabrication conditions.

A thorough examination of the wear tracks generated during the various sample processing methods reveals that for both pin on disk and ball on plate tests the wear mechanism observed were: oxidation, plastic deformation, and abrasion. These results are consistent with those obtained by Sanguedolce et al. [27] in 17-4 PH steel processed by SLM. However, in the case of the lubricated circular wear test, no significant mechanism wear could be detected due to the limited footprint left on the sample. Based on the elemental distribution analysis by EDX conducted on the wear tracks in general, it was observed that the tracks on samples subjected to dry wear, were covered with protective oxide films, Fig. 10. This finding was independent of the manufacturing process used.

In Fig. 11, images obtained by scanning electron microscopy (SEM) are presented, where three main phenomena are observed: delaminations, plastic deformation wear, and the presence of wear particles (debris). These phenomena were observed in both dry wear test samples, regardless of the manufacturing process used. The presence of delaminations and wear particles in the worn area is consistent with the results shown in other previous studies [40,42]. The presence of delamination has been previously observed in stainless steels processed by SLM [35].

On the other hand, Wrought and FFF 17-4 PH SS samples after pin on disk teste showed grooves that show the existence of abrasive wear caused by the dragging of particles along the wear track. These dragged particles accumulate, forming a sort of debris in certain areas of the

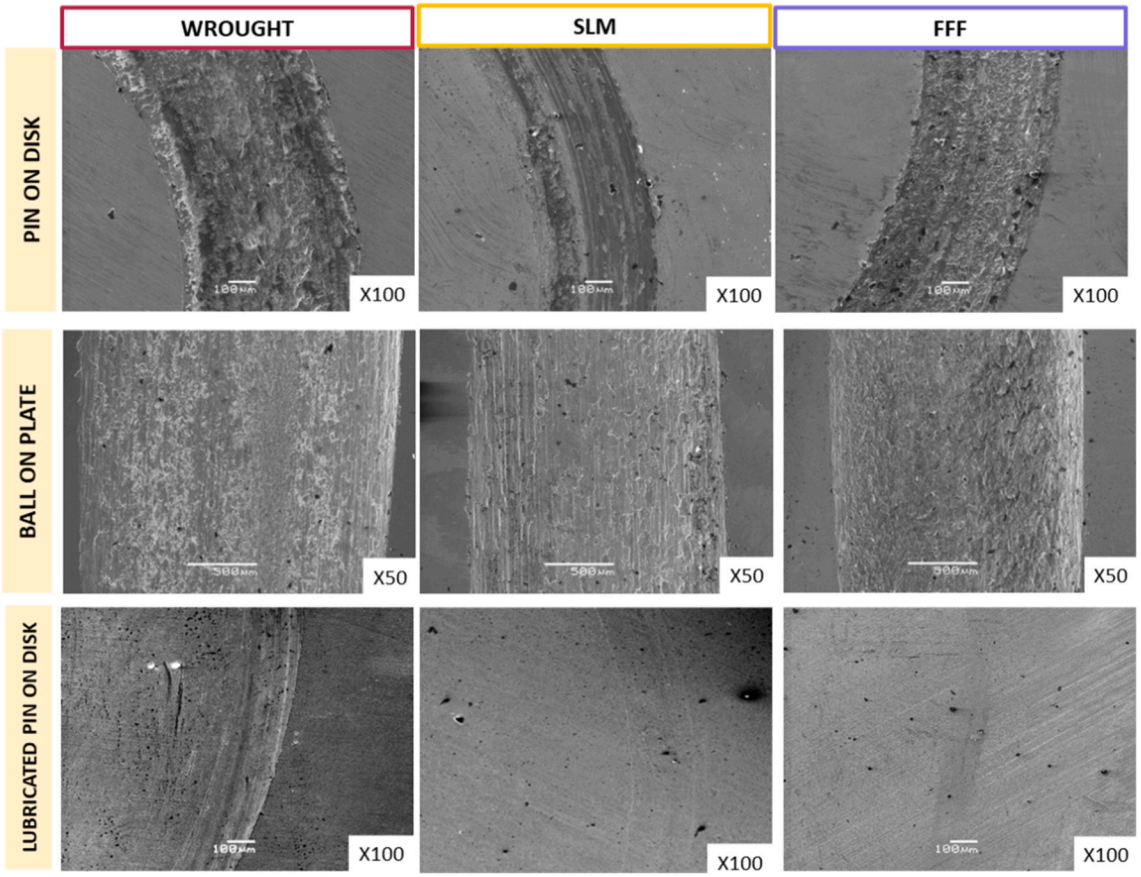

Fig. 9. SEM images depict wear tracks generated on the 17-4 PH material for all three manufacturing processes (wrought, SLM and FFF) and the three tribological tests conducted (pin on disk, ball on plate and lubricated pin on disk).

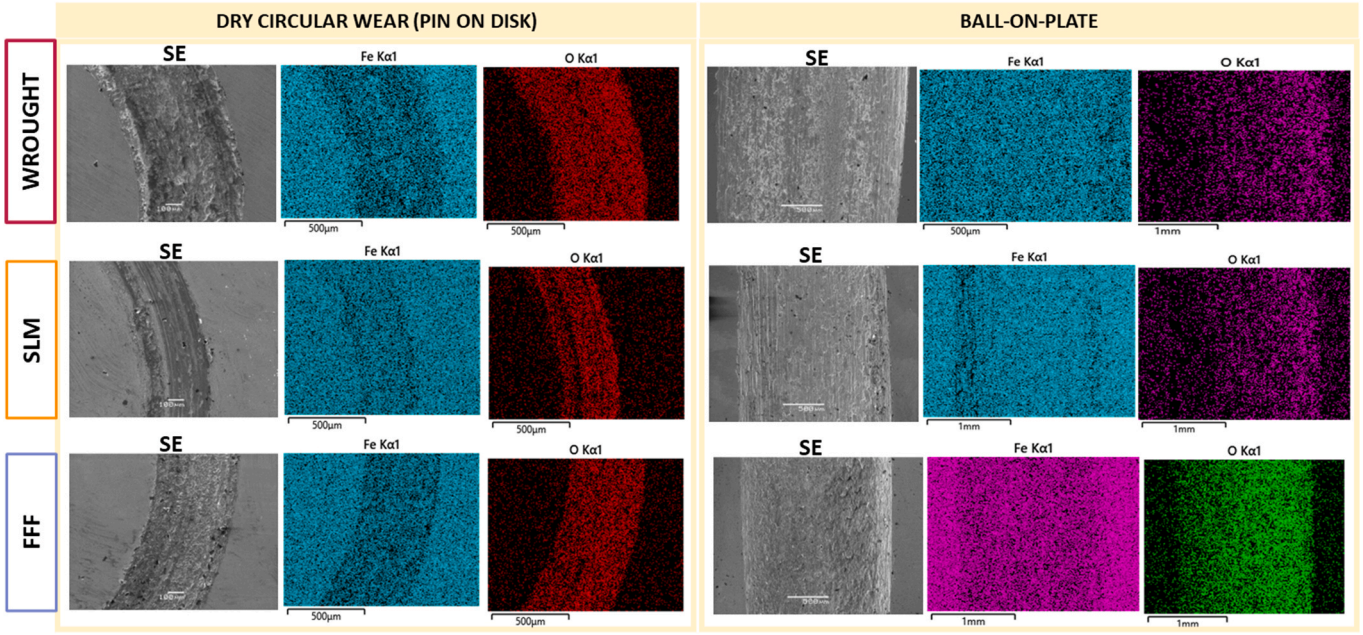

Fig. 10. Distribution maps of wear tracks for each manufacturing process under dry wear and ball-on-plate wear conditions. However, a complete absence of oxide was observed throughout the lubricated wear track. This observation indicates that, in terms of wear protection, all samples exhibited similar behavior and were capable of generating protective oxide films in response to wear.

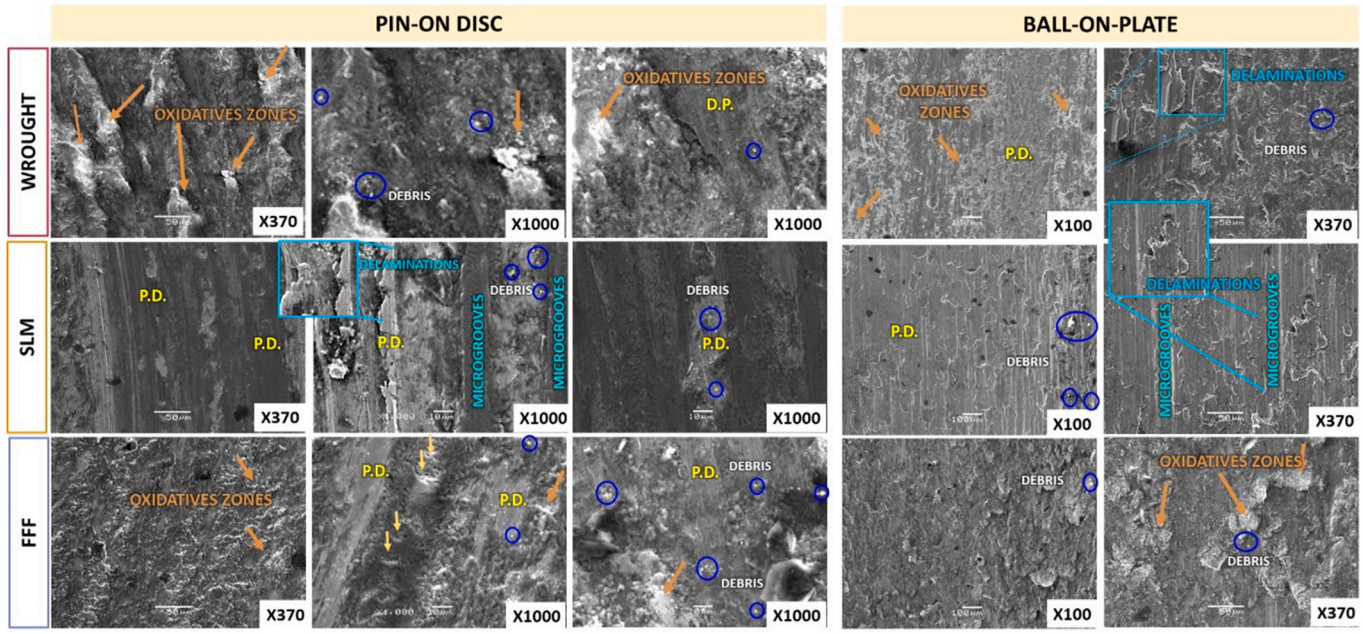

Fig. 11. SEM micrographs of the surface morphology at the pin-on disk and ball-on-plate interfaces produced by different fabrication processes tagging: debris, delaminations, oxidative zones, plastic deformation (P.D.) and microgrooves.

track (indicated by orange arrows as oxidatives zones in Fig. 11).

This behavior suggests that there is detachment of the oxide layer formed on the surface of the samples during the wear process. This suggests that oxidative wear is caused by the periodic removal of the passive film by the slider, followed by the passivation of the exposed metal surface, as indicated in other studies [43]. The presence of a higher amount of oxygen in these accumulated particles supports this phenomenon, as can be observed in the spectrum obtained from one of these areas (Fig. 10).

In the sample processed by SLM, the signs of oxidation are less evident, however, more detailed analysis of a specific area of this wear track reveals distinct composition and morphology of the crests and valleys observed in Fig. 12. These compositional differences are reflected in both the distribution maps and composition tables obtained from the identified zones, revealing disparities in oxygen content among them. The oxygen distribution mapping confirms that the oxidative areas correspond to the microgrooves, as evidenced by a higher density of data points in those regions. This observation is further supported by the composition study conducted at different points on the wear track (1, 2), where the content of O, Fe, and C is displayed for each respective zone.

These microgrooves exhibit typical characteristics of abrasion wear

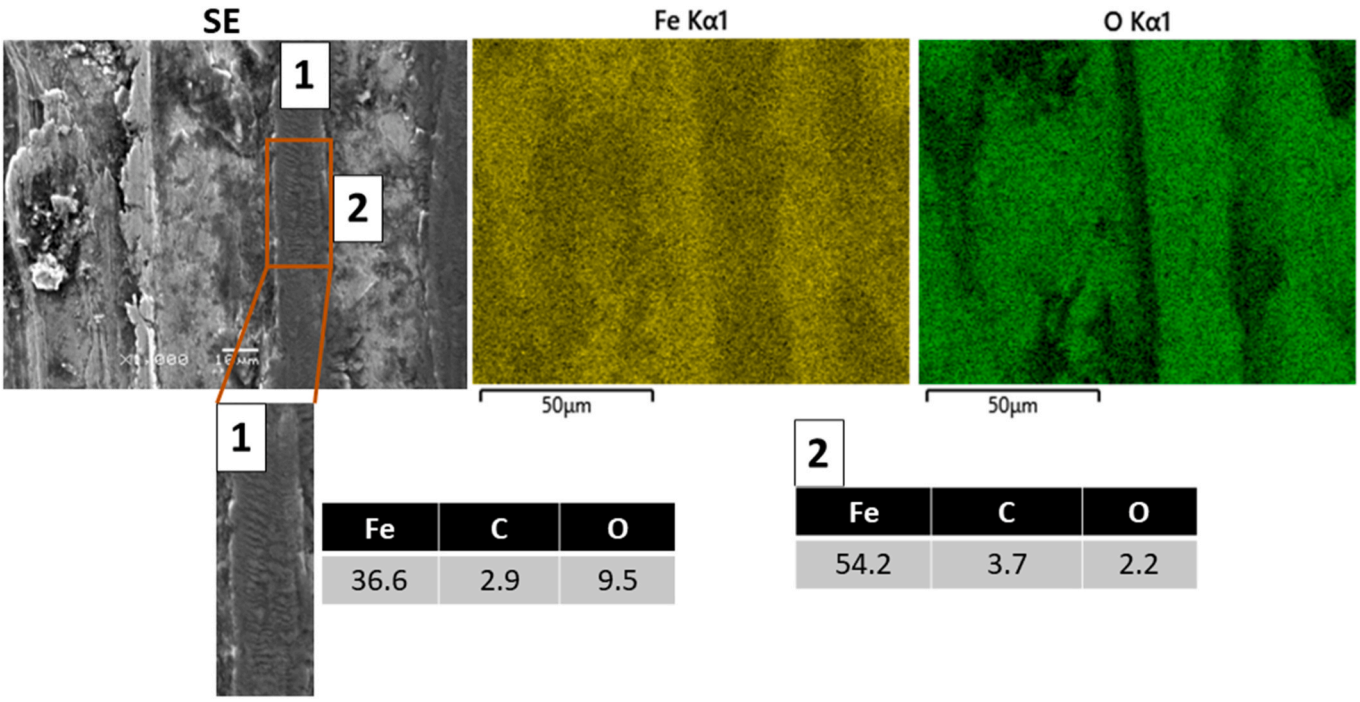

Fig. 12. Evolution of the composition in the wear track produced under dry wear conditions in the SLM processed sample.

promoted by the third body mechanism, known as microcracks, which can be observed in Fig. 12 at point 1 [40]. The results indicate that abrasion wear is more pronounced in FFF and wrought compared to SLM. Conversely, in the SLM process, greater plastic deformation (tagged as P.D.) is observed. This is in line with the work of Tekdir and Yetim [29] who identified the presence of delamination wear on the surface of 316L processed by SLM.

In all cases, particles called *debris* were observed on the surfaces of the wear tracks, as shown in Fig. 11 with blue circles. X-ray spectroscopy analysis of these particles indicates the presence of aluminum in their composition (Fig. 13); therefore, it could correspond to pin particles plastalongside other iron and chromium oxide particles.

On the other hand, the XRD spectrum of the wear debris collected for each sample after the wear tests are shown in Fig. 14. For all samples, the XRD results show that these particles are mostly iron oxide and iron chromium oxide with broad peaks at $2\theta = 15°$ and $30°$. In addition, it was observed peaks associated to α′martensite at $2\theta = 44.7°$ (110) and $64.5°$ (200) and a small shoulder at approximately $40.3°$ that corresponds with Al_2O_3 from the pin. The intensity of the peaks from oxides is higher in the additively manufactured samples (SLM and FFF), while the conventional wrought sample showed peaks with higher intensities associated to the metallic phase, which is consistent with the lower wear resistance obtained in this sample. Finally, the intensity of the peaks that correspond with alumina is higher in the SLM and FFF samples, indicating that due to the higher wear resistance of these samples the wear caused in the alumina pin is higher and, therefore, the debris generated from these samples contained a more substantial amount of alumina compared to the debris from the wrought sample.

4. Conclusions

This work analyses the microstructural, mechanical and tribological

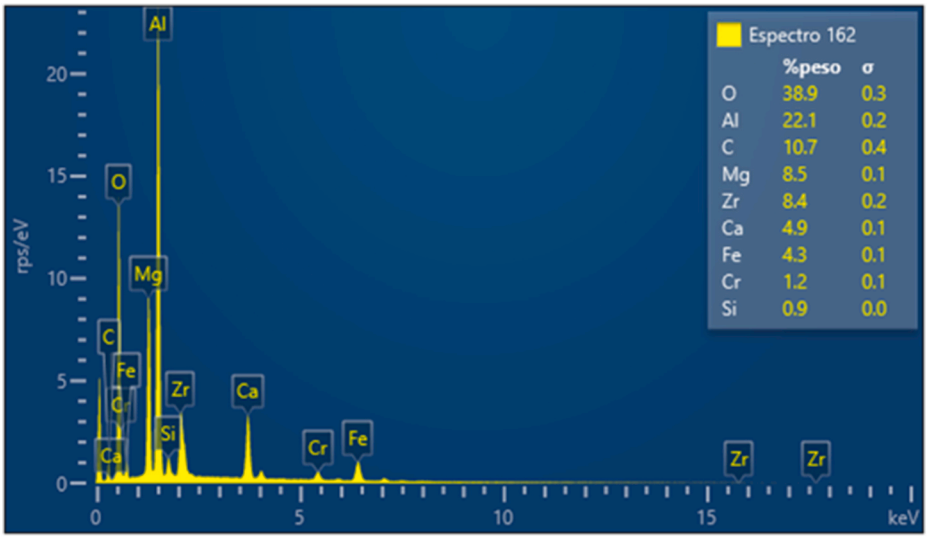

Fig. 13. X-ray spectrum obtained from a wear particle present in the track of the FFF-processed sample.

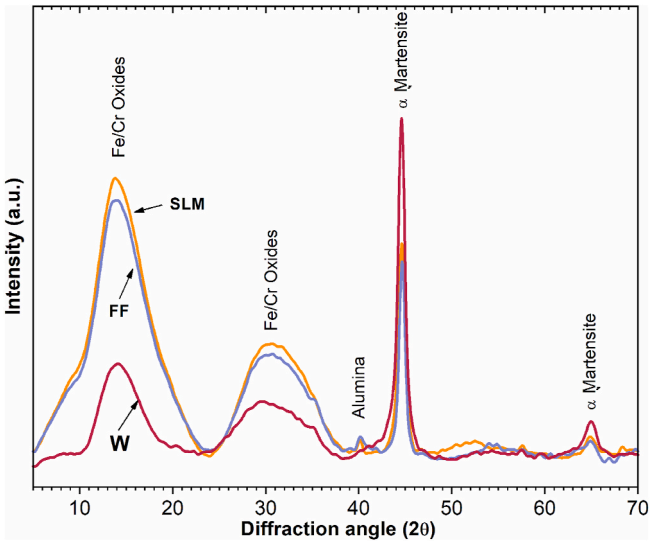

Fig. 14. XRD spectrum of the wear debris for wrought, SLM and FFF samples.

behaviour of 17–4 PH stainless steel specimens fabricated by different AM process, SLM and FFF, in comparison with conventional wrought steel. The following conclusions can be deduced from this study.

1. This study has revealed that additive manufacturing can be successfully used to produce metal components in 17–4 PH SS with comparable and/or even superior properties to those obtained in commercial counterparts.
2. The microstructure of the samples depends on the fabrication process. An adequate selection of the fabrication parameters is essential to obtain full density samples in SLM and FFF fabrication process.
3. For SLM samples, an anisotropic and complex martensite structure with retained austenite was observed, while the FFF steel showed a duplex delta ferrite-martensite microstructure. Moreover, in both AM samples, precipitates rich in Cr, and Nb were detected in as-built condition.
4. The hardness of steels produced by AM is slightly lower than that of conventionally produced counterpart steels. This can be justified by the higher amount of retained austenite/delta ferrite and the lower amount of precipitates of AM specimens compared to heat-treated wrought samples. In addition, residual tensions derived from AM processing could explain the lower ductility of SLM and FFF samples in comparison with wrought steel.
5. For all test conditions, AM 17–4 PH SS showed lower wear rate values and lower coefficients of friction than the reference material, which means that the tribological behaviour of additive manufacturing is superior.
6. The formation and delamination of iron/chromium oxide film was the main wear mechanism in AM specimens. Moreover, abrasive mechanism associated to alumina debris was more visible for wrought SS.

Thus, additive manufacturing could be a promising and reliable technology for the fabrication of 17–4 PH parts, showing a significant improvement in tribological behaviour, and can be especially interesting when the geometry of the pieces has characteristics that difficult the fabrication and/or increase the manufacturing price or even when production runs are relatively small. These results further support the superior wear performance of the additively manufactured samples and highlight the importance of understanding wear mechanisms and material interactions to optimize the wear resistance of engineered components. The wear behavior of the samples is notably influenced by a combination of microstructural factors, hardness, and lubrication conditions, emphasizing the intricate and multifaceted nature of wear resistance in additively manufactured components.

In near future, the tribological study will be extended with other test conditions (steel pin, longer test times, lubrication in ball-on-flat tests) that may give rise to new wear mechanisms.

Moreover, it would be interesting to carry out tribocorrosion studies on 17–4 PH SS in order to compare the behaviour of this material depending on the fabrication process using samples fabricated by other additive manufacturing methods and the wrought as reference.

CRediT authorship contribution statement

Celia García-Hernández: Data curation, Methodology, Visualization, Writing – original draft, Writing – review & editing. **Juan Alfonso Naranjo:** Data curation, Formal analysis, Investigation, Validation, Visualization, Writing – original draft, Writing – review & editing. **María Ángeles Castro-Sastre:** Investigation, Methodology, Writing – original draft, Writing – review & editing. **Cristina Berges:** Data curation, Investigation, Methodology. **A.I. Fernandez-Abia:** Investigation, Methodology, Writing – original draft, Writing – review & editing, Investigation, Methodology. **Fernando Martín-Pedrosa:** Data curation, Funding acquisition, Validation, Writing – original draft. **Gemma Herranz:** Investigation, Methodology, Writing – original draft, Writing – review & editing.

Declaration of competing interest

The authors declare that they have no known competing financial interests or personal relationships that could have appeared to influence the work reported in this paper.

Cristina Garcia-Cabezon reports financial support, administrative support, and article publishing charges were provided by Universidad de Valladolid. Cristina Garcia Cabezon reports a relationship with University of Valladolid that includes: employment. No Conflict of interest.

Data availability

Data will be made available on request.

Acknowledgments

This work was supported by MICINN-FEDER (PID2021-122365OB-I00), «Infraestructuras Red de Castilla y Leon (INFRARED)», JCyL Consejería de Educación - FEDER (VA275P18) and by the pre-doctoral grant [2018/12504], co-financed from the Government of Castilla-La Mancha and the European Union through the European Social Fund.

References

[1] S.S. Tavares, J.S. Corte, J.M. Pardal, Failure of 17-4PH stainless steel components in offshore platforms, in: Handbook of Materials Failure Analysis with Case Studies from the Oil and Gas Industry, Elsevier, 2015, pp. 353–370.
[2] C. Suwanpreecha, A. Manonukul, On the build orientation effect in as-printed and as-sintered bending properties of 17-4PH alloy fabricated by metal fused filament fabrication, RPJ 28 (2022) 1076–1085, https://doi.org/10.1108/RPJ-07-2021-0174.
[3] S. Atatreh, M.S. Alyammahi, H. Vasilyan, T. Alkindi, R.A. Susantyoko, Evaluation of the infill design on the tensile properties of metal parts produced by fused filament fabrication, Results in Engineering 17 (2023) 100954, https://doi.org/10.1016/j.rineng.2023.100954.
[4] H. Ye, X.Y. Liu, H. Hong, Sintering of 17-4PH stainless steel feedstock for metal injection molding, Mater. Lett. 62 (2008) 3334–3336, https://doi.org/10.1016/j.matlet.2008.03.027.
[5] C. Suwanpreecha, A. Manonukul, A review on material extrusion additive manufacturing of metal and how it compares with metal injection moulding, Metals 12 (2022) 429, https://doi.org/10.3390/met12030429.
[6] S. Xu, W.R. Tyson, R. Eagleson, R. Zavadil, Z. Liu, P.-L. Mao, C.-Y. Wang, S.I. Hill, A.A. Luo, Dependence of flow strength and deformation mechanisms in common wrought and die cast magnesium alloys on orientation, strain rate and temperature, J. Magnesium Alloys 1 (2013) 275–282, https://doi.org/10.1016/j.jma.2013.11.003.

[7] O. Miclette, R. Côté, V. Demers, V. Brailovski, Material extrusion additive manufacturing of low-viscosity metallic feedstocks: performances of the plunger-based approach, Addit. Manuf. 60 (2022) 103252, https://doi.org/10.1016/j.addma.2022.103252.
[8] T. LeBrun, T. Nakamoto, K. Horikawa, H. Kobayashi, Effect of retained austenite on subsequent thermal processing and resultant mechanical properties of selective laser melted 17–4 PH stainless steel, Mater. Des. 81 (2015) 44–53, https://doi.org/10.1016/j.matdes.2015.05.026.
[9] T. LeBrun, T. Nakamoto, K. Horikawa, H. Kobayashi, Effect of retained austenite on subsequent thermal processing and resultant mechanical properties of selective laser melted 17–4 PH stainless steel, Mater. Des. 81 (2015) 44–53, https://doi.org/10.1016/j.matdes.2015.05.026.
[10] I. Thawon, T. Fongsamootr, Y. Mona, P. Suttakul, Investigation of the mechanical properties of additively manufactured metal parts with different relative densities, Appl. Sci. 12 (2022) 9915, https://doi.org/10.3390/app12199915.
[11] L.E. Murr, E. Martinez, J. Hernandez, S. Collins, K.N. Amato, S.M. Gaytan, P. W. Shindo, Microstructures and properties of 17-4 PH stainless steel fabricated by selective laser melting, J. Mater. Res. Technol. 1 (2012) 167–177, https://doi.org/10.1016/S2238-7854(12)70029-7.
[12] D.J. Kotecki, T.A. Siewert, WRC-1992 constitution diagram for stainless steel weld metals: a modification of the WRC-1988 diagram, Weld. J. 71 (1992) 171–178.
[13] S. Cheruvathur, E.A. Lass, C.E. Campbell, Additive manufacturing of 17-4 PH stainless steel: post-processing heat treatment to achieve uniform reproducible microstructure, J. Miner. Met. Mater. Soc. 68 (2016) 930–942, https://doi.org/10.1007/s11837-015-1754-4.
[14] B. Clausen, D.W. Brown, J.S. Carpenter, K.D. Clarke, A.J. Clarke, S.C. Vogel, J. D. Bernardin, D. Spernjak, J.M. Thompson, Deformation behavior of additively manufactured GP1 stainless steel, Mater. Sci. Eng. 696 (2017) 331–340, https://doi.org/10.1016/j.msea.2017.04.081.
[15] N. Maharjan, W. Zhou, Y. Zhou, N. Wu, Decarburization during laser surface processing of steel, Appl. Phys. A 124 (2018) 1–9, https://doi.org/10.1007/s00339-018-2104-5.
[16] S. Pasebani, M. Ghayoor, S. Badwe, H. Irrinki, S.V. Atre, Effects of atomizing media and post processing on mechanical properties of 17-4 PH stainless steel manufactured via selective laser melting, Addit. Manuf. 22 (2018) 127–137, https://doi.org/10.1016/j.addma.2018.05.011.
[17] Z. Hu, H. Zhu, H. Zhang, X. Zeng, Experimental investigation on selective laser melting of 17-4PH stainless steel, Opt Laser. Technol. 87 (2017) 17–25, https://doi.org/10.1016/j.optlastec.2016.07.012.
[18] A. Yadollahi, M. Mahmoudi, A. Elwany, H. Doude, L. Bian, J.C. Newman, Effects of crack orientation and heat treatment on fatigue-crack-growth behavior of AM 17-4 PH stainless steel, Eng. Fract. Mech. 226 (2020) 106874, https://doi.org/10.1016/j.engfracmech.2020.106874.
[19] Y. Abe, T. Kurose, M.V.A. Santos, Y. Kanaya, A. Ishigami, S. Tanaka, H. Ito, Effect of layer directions on internal structures and tensile properties of 17-4PH stainless steel parts fabricated by fused deposition of metals, Materials 14 (2021), https://doi.org/10.3390/ma14020243.
[20] D. Godec, S. Cano, C. Holzer, J. Gonzalez-Gutierrez, Optimization of the 3D printing parameters for tensile properties of specimens produced by fused filament fabrication of 17-4PH stainless steel, Materials 13 (2020), https://doi.org/10.3390/ma13030774.
[21] C. Tosto, J. Tirillò, F. Sarasini, G. Cicala, Hybrid metal/polymer filaments for fused filament fabrication (FFF) to print metal parts, Appl. Sci. 11 (2021) 1444, https://doi.org/10.3390/app11041444.
[22] A. Kudzal, B. McWilliams, C. Hofmeister, F. Kellogg, J. Yu, J. Taggart-Scarff, J. Liang, Effect of scan pattern on the microstructure and mechanical properties of Powder Bed Fusion additive manufactured 17-4 stainless steel, Mater. Des. 133 (2017) 205–215, https://doi.org/10.1016/j.matdes.2017.07.047.
[23] H.R. Lashgari, C. Kong, E. Adabifiroozjaei, S. Li, Microstructure, post thermal treatment response, and tribological properties of 3D printed 17-4 PH stainless steel, Wear 456–457 (2020) 203367, https://doi.org/10.1016/j.wear.2020.203367.
[24] Y. Yang, Y. Zhu, M.M. Khonsari, H. Yang, Wear anisotropy of selective laser melted 316L stainless steel, Wear 428–429 (2019) 376–386, https://doi.org/10.1016/j.wear.2019.04.001.
[25] K.C. Sanjeev, P.D. Nezhadfar, C. Phillips, M.S. Kennedy, N. Shamsaei, R.L. Jackson, Tribological behavior of 17–4 PH stainless steel fabricated by traditional manufacturing and laser-based additive manufacturing methods, Wear 440–441 (2019) 203100, https://doi.org/10.1016/j.wear.2019.203100.
[26] M. Naim, M. Chemkhi, A. Alhussein, D. Retraint, Effect of post-treatments on the tribological and corrosion behavior of 17–4PH stainless steel processed via fused filament fabrication, Additive Manufacturing Letters 7 (2023) 100158, https://doi.org/10.1016/j.addlet.2023.100158.
[27] M. Sanguedolce, J. Zekonyte, M. Alfano, Wear of 17-4 PH stainless steel patterned surfaces fabricated using selective laser melting, Appl. Sci. 11 (2021) 9317, https://doi.org/10.3390/app11199317.
[28] H. Li, M. Ramezani, M. Li, C. Ma, J. Wang, Tribological performance of selective laser melted 316L stainless steel, Tribol. Int. 128 (2018) 121–129, https://doi.org/10.1016/j.triboint.2018.07.021.
[29] H. Tekdir, A.F. Yetim, Additive manufacturing of multiple layered materials (Ti6Al4V/316L) and improving their tribological properties with glow discharge surface modification, Vacuum 184 (2021) 109893, https://doi.org/10.1016/j.vacuum.2020.109893.
[30] J.A. Naranjo, C. Berges, R. Campana, G. Herranz, Rheological and mechanical assessment for formulating hybrid feedstock to be used in MIM & FFF, Results in Engineering 19 (2023) 101258, https://doi.org/10.1016/j.rineng.2023.101258.
[31] C. Garcia-Cabezon, M.A. Castro-Sastre, A.I. Fernandez-Abia, M.L. Rodriguez-Mendez, F. Martin-Pedrosa, Microstructure–hardness–corrosion performance of 17–4 precipitation hardening stainless steels processed by selective laser melting in comparison with commercial alloy, Met. Mater. Int. 28 (2022) 2652–2667, https://doi.org/10.1007/s12540-021-01155-8.
[32] G02 Committee, ASTM G99-17. Test Method for Wear Testing with a Pin-On-Disk Apparatus, ASTM International, West Conshohocken, PA, 2017.
[33] G02 Committee, ASTM G133-22. Test Method for Linearly Reciprocating Ball-on-Flat Sliding Wear, ASTM International, West Conshohocken, PA, 2022.
[34] C.N. Hsiao, C.S. Chiou, J.R. Yang, Aging reactions in a 17-4 PH stainless steel, Mater. Chem. Phys. 74 (2002) 134–142, https://doi.org/10.1016/S0254-0584(01)00460-6.
[35] T. Yetim, H. Tekdir, M. Taftalı, K. Turalıoğlu, A.F. Yetim, Synthesis and characterisation of single and duplex ZnO/TiO 2 ceramic films on additively manufactured bimetallic material of 316L stainless steel and Ti6Al4V, Surf. Topogr. Metrol. Prop. 11 (2023) 24005, https://doi.org/10.1088/2051-672X/accf6c.
[36] S. Sarkar, S. Mukherjee, C.S. Kumar, A. Kumar Nath, Effects of heat treatment on microstructure, mechanical and corrosion properties of 15-5 PH stainless steel parts built by selective laser melting process, J. Manuf. Process. 50 (2020) 279–294, https://doi.org/10.1016/j.jmapro.2019.12.048.
[37] Folgarait Zitelli, Di Schino, Laser powder bed fusion of stainless steel grades: a review, Metals 9 (2019) 731, https://doi.org/10.3390/met9070731.
[38] A. Yadollahi, N. Shamsaei, S.M. Thompson, A. Elwany, L. Bian, Effects of building orientation and heat treatment on fatigue behavior of selective laser melted 17-4 PH stainless steel, Int. J. Fatig. 94 (2017) 218–235, https://doi.org/10.1016/j.ijfatigue.2016.03.014.
[39] B. Hutchinson, D. Lindell, M. Barnett, Yielding behaviour of martensite in steel, ISIJ Int. 55 (2015) 1114–1122, https://doi.org/10.2355/isijinternational.55.1114.
[40] J.D. Bressan, D.P. Daros, A. Sokolowski, R.A. Mesquita, C.A. Barbosa, Influence of hardness on the wear resistance of 17-4 PH stainless steel evaluated by the pin-on-disc testing, J. Mater. Process. Technol. 205 (2008) 353–359, https://doi.org/10.1016/j.jmatprotec.2007.11.251.
[41] S.H. Teoh, R. Thampuran, W. Seah, Coefficient of friction under dry and lubricated conditions of a fracture and wear resistant P/M titanium-graphite composite for biomedical applications, Wear 214 (1998) 237–244, https://doi.org/10.1016/S0043-1648(97)00231-7.
[42] K.-H. Gahr, Wear by hard particles, Tribol. Int. 31 (1998) 587–596, https://doi.org/10.1016/S0301-679X(98)00079-6.
[43] M. Esfandiari, H. Dong, The corrosion and corrosion–wear behaviour of plasma nitrided 17-4PH precipitation hardening stainless steel, Surf. Coating. Technol. 202 (2007) 466–478, https://doi.org/10.1016/j.surfcoat.2007.06.069.